

Measurement of the noise generated by wall-mounted airfoils of different thickness

Thomas F. Geyer*

Brandenburg University of Technology Cottbus - Senftenberg, 03046 Cottbus, Germany

Danielle J. Moreau†

The University of New South Wales, Sydney NSW 2052, Australia

Jens Giesler‡ Philipp M. Hall§

Brandenburg University of Technology Cottbus - Senftenberg, 03046 Cottbus, Germany

Ennes Sarradj¶

Technische Universität Berlin, 10587 Berlin, Germany

Con J. Doolan||

The University of New South Wales, Sydney NSW 2052, Australia

The flow around a wall-mounted finite airfoil with natural transition can lead to complex tonal characteristics in the corresponding aeroacoustic noise spectra. While many of the flow features and noise generating mechanisms are well understood, there are still open questions, for example regarding the influence of the airfoil shape. In the present paper, the influence of the thickness of a wall-mounted finite airfoil on the noise generation is examined experimentally. To this end, detailed measurements were performed on a NACA0012 airfoil and a NACA0018 airfoil in an open jet aeroacoustic wind tunnel at various flow speeds and angles of attack. This includes acoustic measurements with a planar microphone array as well as measurements of the surface pressure fluctuations using flush-mounted pressure capsules. In addition, surface flow visualization experiments were conducted on the NACA0012 airfoil. The results show that the thickness of the airfoil has a notable influence on the tonal noise generation, which is visible both in the sound pressure level spectra as well as in the wall pressure spectra. At small geometric angles of attack and high flow speeds, the thinner NACA0012 generates a strong tone with weaker side tones, whereas the NACA0018 generates a set of equispaced tones. At higher angles the NACA0012 does not radiate tonal noise, while the NACA0018 now generates this strong tone with weaker side tones.

I. Introduction

The noise generation by two-dimensional airfoils is a classical problem in aeroacoustics, which can occur due to the implementation of lifting surfaces in a variety of technical applications such as fans, wind turbines and aircraft wings. Depending on the flow conditions and the shape and dimensions of the airfoil, several noise generation mechanisms may develop [1], and the resulting noise spectrum can feature both broadband and tonal characteristics. For example, tonal trailing edge noise can be generated when the chord based

*Research Assistant, Technical Acoustics Group, Brandenburg University of Technology Cottbus - Senftenberg, Germany.

†Lecturer, School of Mechanical and Manufacturing Engineering, AIAA member.

‡former Research Assistant, Technical Acoustics Group, Brandenburg University of Technology Cottbus - Senftenberg, Germany.

§Master Student, Technical Acoustics Group, Brandenburg University of Technology Cottbus - Senftenberg, Germany.

¶Professor, Institute of Fluid Mechanics and Engineering Acoustics, Technical University Berlin, Germany.

||Associate Professor, School of Mechanical and Manufacturing Engineering, AIAA Senior member.



Figure 1. Airfoils used in the present study

Reynolds number does not exceed a critical value and hence no boundary layer transition occurs [2–5]. It was first discovered by Paterson et al. [2] that airfoils that shed vortices in a laminar flow generate a very distinctive spectral pattern, which is known as a “ladder-type” structure. Thereby, the farfield spectrum consists of a primary tone, whose frequency increases with $U^{0.8}$ (with U being the flow speed) over a finite range of speeds, before “jumping” to another rung of the ladder and following a new $U^{0.8}$ power law. In addition, the spectra contain side tones which increase with $U^{1.5}$, thus building the rungs of the ladder.

If the airfoils are not only two-, but three-dimensional, further noise source mechanisms develop at the airfoil tip, which may additionally lead to strong tonal noise contributions [6–9].

The principal objective of the present study is to examine the noise generation and surface flow characteristics of wall-mounted finite airfoils with varying thickness. To this end, a set of experiments was performed in an open jet wind tunnel. In addition to acoustic microphone array measurements, wall-pressure fluctuations were measured and surface flow visualizations were performed.

II. Materials and Methods

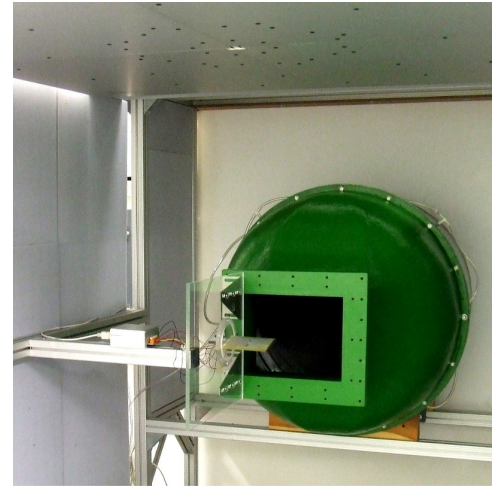
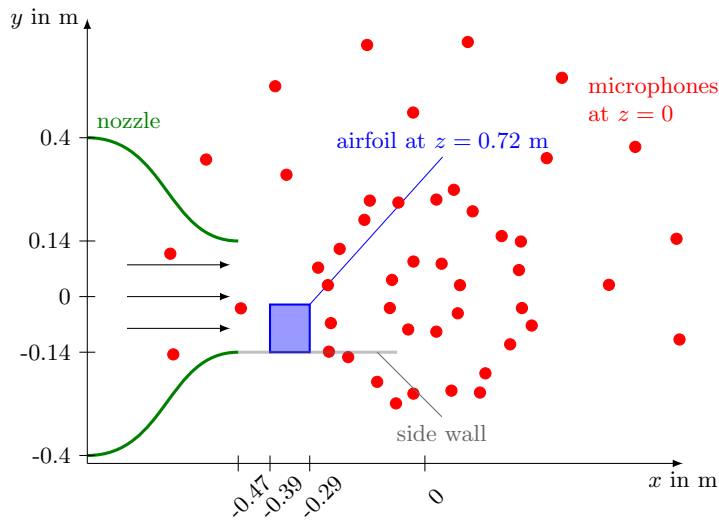
II.A. Wind Tunnel and Airfoil Models

All experiments were performed in the small aeroacoustic wind tunnel at the Brandenburg University of Technology in Cottbus [10], using a nozzle with a rectangular exit area of $0.23 \text{ m} \times 0.28 \text{ m}$. In order to provide a quasi-anechoic environment, the open test section of the wind tunnel is surrounded by a cabin with absorbing side walls for frequencies approximately above 125 Hz. Two different airfoils were tested in the study, a NACA0012 and a NACA0018, which are shown schematically in Figure 1. Both had a chord length c_l of 0.1 m and a span width b of 0.12 m, resulting in an aspect ratio of 1.2. The maximum thickness of the airfoils is 12 mm for the NACA0012 and 18 mm for the NACA0018. At one end, the airfoils were mounted to a side wall, while the tip of the airfoil at the other end was flat. The distance between nozzle and airfoil leading edge was 75 mm. No tripping tape was applied to the airfoil surface, allowing for natural transition. Figure 2 shows a schematic and a photograph of the setup.

Prior to the experiments, the thickness of the boundary layer at the position of the airfoil leading edge (but without the airfoil in place) was measured via constant temperature anemometry using a Dantec P15 single wire boundary layer probe. Figure 3 shows the velocity profiles and the boundary layer thickness δ , normalized by the span width b , as a function of flow speed. The boundary layer thickness takes values between approximately 16 mm at low flow speeds and 9 mm at the highest flow speeds, which is about 14 % to 8 % of the airfoil span.

II.B. Microphone Array and Data Processing

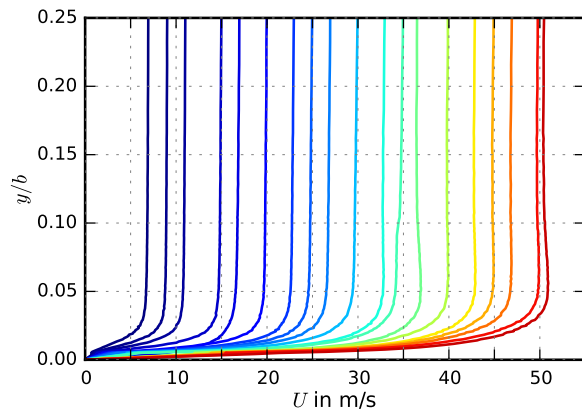
The acoustic measurements were performed using a planar 47-channel microphone array, positioned above the airfoil and outside of the flow. The position of the microphones is indicated in Figure 2(a). The data were acquired with a sampling frequency of 51.2 kHz and a duration of 40 s using a National Instruments 24 Bit multichannel measurement system. In post processing, the data were transferred to the frequency domain using a Fast Fourier Transformation (FFT) on 50 % overlapping blocks with a size of 16,384 samples and Hanning windowing. After averaging, the resulting cross-spectral matrices were further processed with the CLEAN-SC deconvolution algorithm [11] to remove the influence of the array-specific point spread function. This was done on a fully three-dimensional focus grid. This grid has a streamwise extent of 0.57 m, a spanwise extent of 0.4 m and a vertical extent of 0.3 m with a resolution of 0.01 m, resulting in 73,718 grid



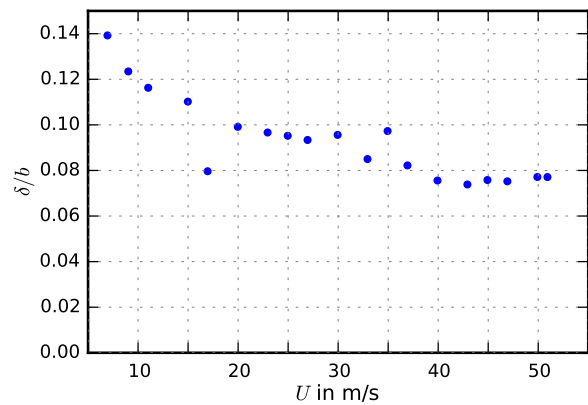
(a) Schematic (top view)

(b) Photograph

Figure 2. Experimental setup inside the aeroacoustic wind tunnel



(a) Velocity profiles



(b) Boundary layer thickness

Figure 3. Velocity profiles and thickness of the wall boundary layer at the position of the airfoil leading edge

points. Finally, in order to obtain the sound pressures generated by the airfoil, those noise contributions were integrated that originate from a three-dimensional sector containing the airfoil, but no potential extraneous noise sources like the nozzle. The data were then converted to power spectral densities L_p re $20 \mu\text{Pa}$.

II.C. Surface Pressure Measurements

Simultaneously to the acoustic measurements, wall pressure fluctuations were measured on the upper surface of the airfoils. This was done using six flush mounted electret microphone cartridges of the type Panasonic WM-61. They were aligned in streamwise direction at $x/c_l = 0.2, 0.32, 0.44, 0.56, 0.68, 0.8$ along a line at midspan (see Figure 4). As for the acoustic measurements, the wall pressures were acquired with a sampling frequency of 51.2 kHz and a duration of 40 s. Again, the time data were transferred to the frequency domain using an FFT with the same settings as for the acoustic data, and power spectral densities were calculated using a reference value of $20 \mu\text{Pa}$.

At low frequencies, it was observed that all spectra of surface pressure fluctuations feature a very sharp peak at exactly 10 kHz which is not generated by the flow, but is an artefact from the signal processing electronics. This peak was removed from most of the wall pressure spectra shown in this paper.

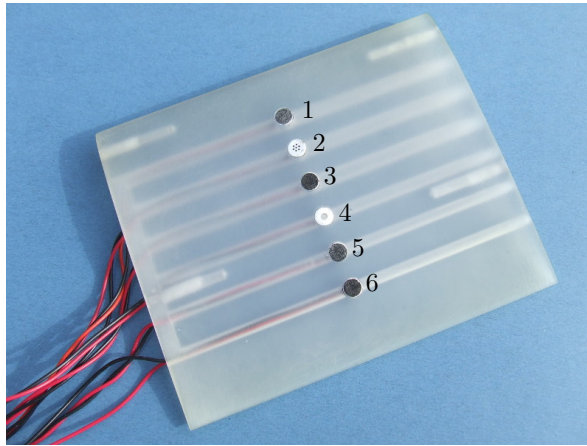


Figure 4. Photograph of the NACA0012 airfoil equipped with electret capsules

Since the airfoils of the present study are the same models used in a previous study by Giesler and Sarradj on turbulence interaction noise [13], the wall pressure sensors are not placed at locations specifically suited for measurements on finite airfoils. For example, sensor locations along a spanwise line in a close proximity to the trailing edge or locations close to the airfoil tip would be favorable, but are not available in the present study. However, this will be the subject of future work.

II.D. Flow Visualization

To allow for basic conclusions on the flow phenomena occurring at a wall-mounted airfoil, additional visualizations of the flow over the surface of a wall-mounted NACA0012 airfoil of the same dimensions, but without the flush-mounted electret capsules, were obtained. For the visualization, a mixture of methylated spirit and talcum powder is applied to the airfoil surface. When the flow is turned on, the methylated spirit evaporates, leaving the talcum powder aligned with the streamlines over the surface of the airfoil.

III. Results

In total, acoustic and wall-pressure measurements were performed at angles of attack of -20° , -15° , -12° , -9° , -6° , -3° , 0° , 3° , 6° , 9° , 12° , 15° , 20° , 25° and 30° and 20 velocities between 6.9 m/s and 52.9 m/s, but for brevity results will only be shown for selected angles of attack. Flow visualization experiments were only performed at zero angle of attack and a reduced number of flow speeds.

III.A. Noise Generation

As an example, Figure 5 shows sound pressure level spectra for six different angles of attack, obtained at two flow speeds of approximately 35 m/s (Figure 5(a)) and 50 m/s (Figure 5(b)). It is instantly visible that the airfoil thickness has a strong effect on the generation of tonal noise: At the lower flow speed and zero angle of attack, the NACA0012 generates several equispaced tones at frequencies between 2 kHz and 3 kHz, while the noise from the NACA0018 has a broadband character without any tones. At the higher flow speed of 50 m/s, the tones from the NACA0012 have nearly disappeared, leaving only very small, equispaced ripples. At an increased geometric angle of 6° , the NACA0012 shows a single, very strong tone at a frequency of about 2150 Hz and a second tone that seems to be the first harmonic of the first tone, since it appears at roughly twice the frequency of the first tone, at the lower speed of 35 m/s. At the higher flow speed of 50 m/s, the spectrum of the NACA0012 features a group of non-equispaced tones. The NACA0018, however, shows a set of equispaced tones with considerably lower amplitude at both flow speeds. Further increasing the angle to 12° reveals no tonal noise for the NACA0012 airfoil, but two strong tones for the NACA0018 airfoil. The first tone appears at a frequency of 3,060 Hz at 35 m/s and at 4,430 Hz at 50 m/s. Again the second tone seems to be the harmonic of the first tone. At 20° angle of attack, neither the NACA0012 nor the NACA0018 generate tonal noise. Since the airfoils are both symmetric, it can be expected that the

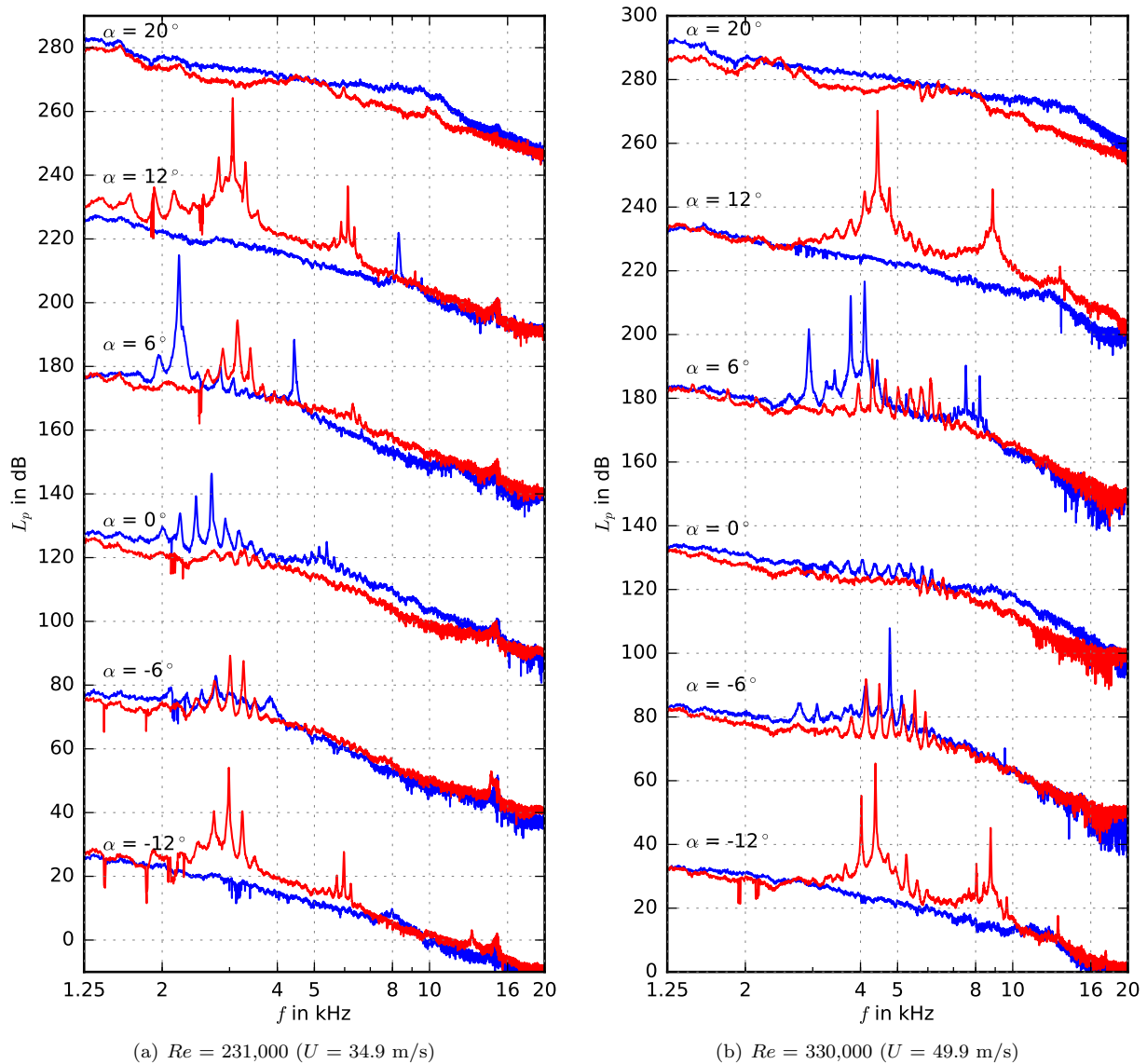


Figure 5. Sound pressure level spectra at different angles of attack, ■ NACA0012, ■ NACA0018 (Spectra at $\alpha > -12^\circ$ have been offset by 50, 100, 150, 200 and 250 dB.)

spectra obtained at negative angles of attack are basically identical to those obtained at positive angles of the same absolute value, which is confirmed by Figure 5.

Figures 6 and 7 show corresponding spectral maps of the measured sound pressure levels as a function of flow speed and frequency for geometric angles of attack of 0° , 3° , 6° , 9° , 12° and 20° . In addition, Figures 8 through 13 show sound maps at the same angles of attack for selected third octave bands, obtained using common delay-and-sum beamforming [12]. The dynamic range of these maps is very small in order to better visualize the location of the major noise source.

Basically, the spectral maps together with the sound maps confirm the findings from the spectra shown in Figure 5, but also give a more general understanding of the generated noise. At zero angle of attack (Figure 6(a)), the NACA0012 only creates some tones in a range of low to medium frequencies from about 1 kHz to 2.5 kHz at flow speeds up to approximately 35 m/s. At higher flow speeds, no tonal noise is generated. This can be assumed to be due to the nature of the boundary layer at the position of the trailing edge. The boundary layer will still be laminar at low flow speeds (and hence tones are created) while it will

be fully turbulent due to natural transition at the higher flow speeds. In accordance, the dominating sound sources shown in Figure 8 for a high flow speed of about 50 m/s are stretched along the trailing edge (with the exception of a small region close to the wall junction). In addition, the sound map obtained at a third octave band with a center frequency of 4 kHz shows a second, somewhat weaker source at the junction of the wall and the leading edge. This is due to the interaction of the turbulent boundary layer at the wall and the leading edge. At this angle of attack, the NACA0018 only generates broadband noise (Figure 7(a)), coming from a source that is stretched along the complete trailing edge. No leading edge source is visible for the NACA0018, since turbulence interaction noise can be expected to contribute less for thicker airfoils. At an angle of attack of 3° , the NACA0012 generates a strong tone and its first harmonic for flow speeds approximately greater than 15 m/s. At the frequency band containing this tone, the corresponding sound maps show a strong source at the trailing edge near the tip (Figure 9). Also noticeable in the spectral map for this angle of attack is a sudden change in the primary tone frequency at a flow speed around 35 m/s, which corresponds to a jump to a higher rung of the frequency ladder. The NACA0018 only generates broadband noise at this angle, again generated by a source extended along almost the complete trailing edge (with the exception of a small region close to the wall junction). At 6° angle of attack, the sound maps in Figure 10 show a trailing edge noise source close to the tip for both airfoils. However, the spectral map shown in Figure 7(c) clearly shows a set of several closely spaced tones for the NACA0018, which are consistent with the set of equispaced tones seen in the spectra shown in Figure 5(b). The NACA0012 again produces one single peak at medium frequencies between 1.6 kHz and 3 kHz as well as the first harmonic of this tone at high frequencies. When the angle of attack is further increased to 9° , the NACA0012 only generates tones at flow speeds approximately above 45 m/s, which are again generated by a source close to the tip at the trailing edge. At lower flow speeds, the NACA0012 generates only broadband noise. The sound pressure level spectra of the NACA0018, however, feature strong tonal peaks (and their first harmonics) at this angle, which again are coming from a trailing edge noise source located close to the tip. Basically, the spectral map obtained for the NACA0018 looks similar at the next higher geometric angle of attack of 12° , with strong tones generated by a source close to the airfoil tip. The spectra generated by the NACA0012 mainly consist of broadband noise at this angle of attack. The corresponding sound maps (see Figure 12) show a strong noise source stretched along the complete trailing edge of the NACA0012. In addition, the noise source generated by the interaction of the wall boundary layer and the leading edge is visible. At a very high geometric angle of attack of 20° , both airfoils generate broadband noise without any visible tones. Interestingly, this noise is not generated by a source extended along the trailing edge (as seen previously for the broadband noise), but by a source located directly at the trailing edge - tip junction.

Basically, the results from the acoustic measurements can be summarized as follows: With the exception of a minor contribution of leading edge noise found at the thinner NACA0012, the noise of both airfoils of the present study is generated by sources located at the trailing edge. At moderate angles of attack from approximately 0° to 12° , the generated tonal noise mostly originates from a noise source located close to the tip of the airfoil, whereas the broadband noise is generated by sources that are stretched along the trailing edge. Thereby, the appearance of the tones is different for the two airfoils. At 6° angle of attack and high flow speeds, the NACA0012 generates a dominant tone with weaker side tones, while the NACA0018 generates a set of equispaced tones of lower amplitude. At 12° , the NACA0012 does not emit tonal noise, but the spectrum of the NACA0018 now features a strong tone with weaker side tones. At high angles of attack (20° to 30°), both airfoils emit broadband noise, which is generated by noise sources at the tip of the airfoils. Interestingly, the NACA0018 shows these sources to be at midchord rather than at the trailing edge for higher frequencies. In general, measurements on even thicker airfoils, such as a NACA0024, would be useful to investigate whether the examined trends continue even further.

III.B. Flow Visualization Results

Figure 14 shows the results from the flow visualization experiments for the NACA0012 at an angle of attack of 0° . Due to the fact that no tripping tape was applied, a noticeable region of separation is visible close to the trailing edge and the tip region of the airfoil. The spanwise extent of this region decreases with increasing flow speed and its location shifts towards the tip. In addition, the figures show that the amount of flow over the tip of the airfoil also increases with increasing flow speed. At the highest Reynolds numbers (297,000 and 330,000) the tip flow even seems to disrupt and perturb the flow separation region.

At zero angle of attack, the spectral map obtained for the NACA0012 (Figure 6(a)) shows tonal noise sources in a frequency region from 1 kHz to 2.5 kHz at flow speeds from about 15 m/s to 35 m/s. This

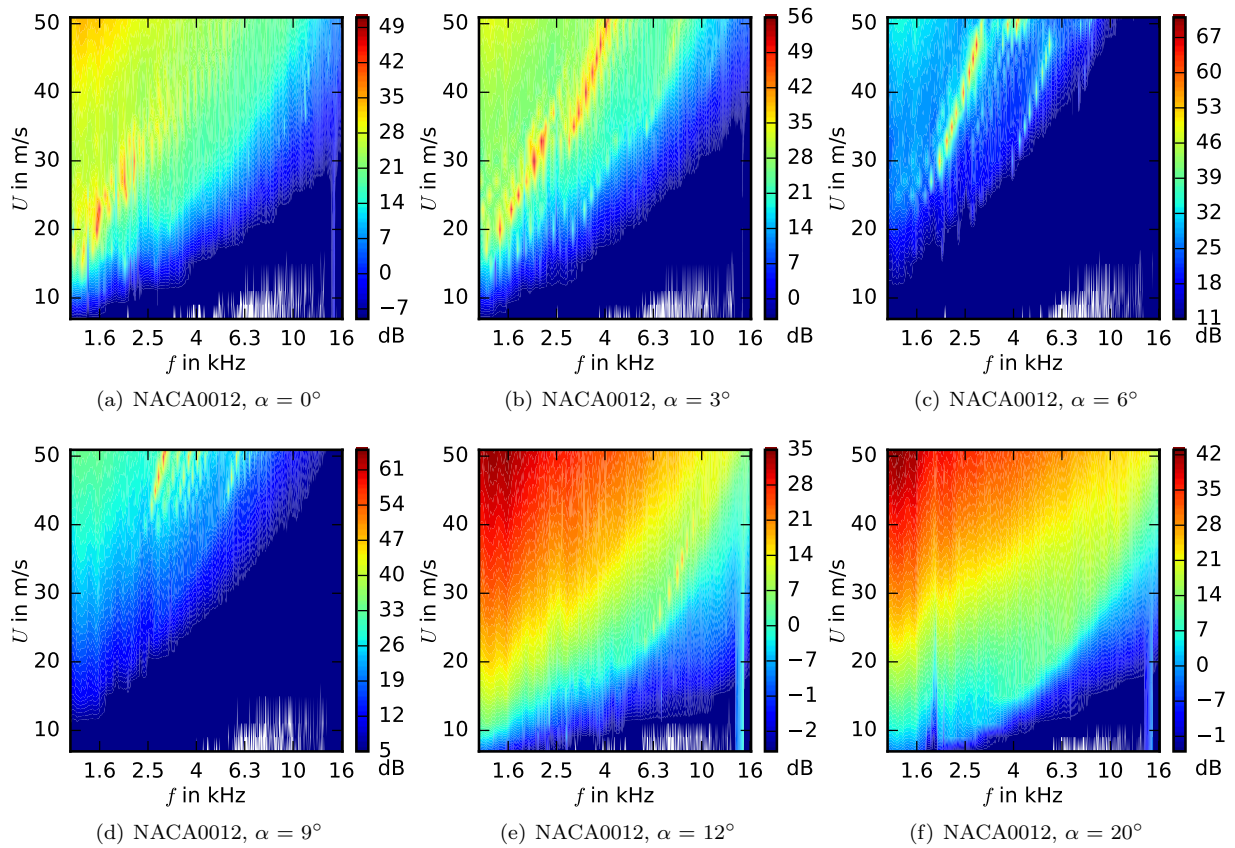


Figure 6. Sound pressure level spectra obtained for the NACA0012 airfoil at different angles of attack as a function of flow speed and frequency

corresponds to the range of flow speeds where Figure 14 shows a clear region of separation, which is a necessary condition for tonal noise generation (interestingly, sound maps for the tonal noise at these low flow speeds show a source at the trailing edge extended along nearly the whole span except for the tip region).

With regard to the wall pressure measurements it can be concluded that at low flow speeds the separation region extends over the spanwise center of the airfoil. Hence it is likely that signals from the pressure sensors close to the trailing edge contain characteristics related to this flow separation.

III.C. Results of Surface Pressure Measurements

Figure 15 shows surface pressure spectra measured by the sensor closest to the trailing edge (sensor 6, at $x/c_l = 0.8$) for both the NACA0012 and the NACA0018 at angles of attack matching those from Figure 5. As discussed in the previous section, at an angle of attack of 0° the NACA0012 generates tonal noise at low flow speeds (Figure 6(a)), which is related to a region of separation on the surface close to the trailing edge, extending over a large part of the airfoil along the span (Figure 14). The wall pressure spectra for this airfoil (Figure 15(a)) at zero angle of attack now show narrow peaks at frequencies between approximately 400 Hz and 800 Hz at flow speeds below 20 m/s. Similar peaks observed in wall-pressure spectra measured by Garcia-Sagrado and Hynes [14] were found to be related to periodic vortical structures in the separated shear layer. They stated that these maxima are associated with Tollmien-Schlichting instability waves in the laminar boundary layer that interact with Kelvin-Helmholtz instabilities from the separated shear layer. If it is assumed that the peaks in the wall pressure spectra shown in Figure 15 will be radiated as tonal noise when they reach the trailing edge, the results from the wall pressure measurements confirm the conclusions from the corresponding acoustic measurements. The absence of such peaks in the wall pressure spectra at higher flow speeds up to approximately 35 m/s, which would be anticipated based on the spectral map shown in Figure 6(a), can be explained by the fact that the separation region then shifts closer towards the airfoil

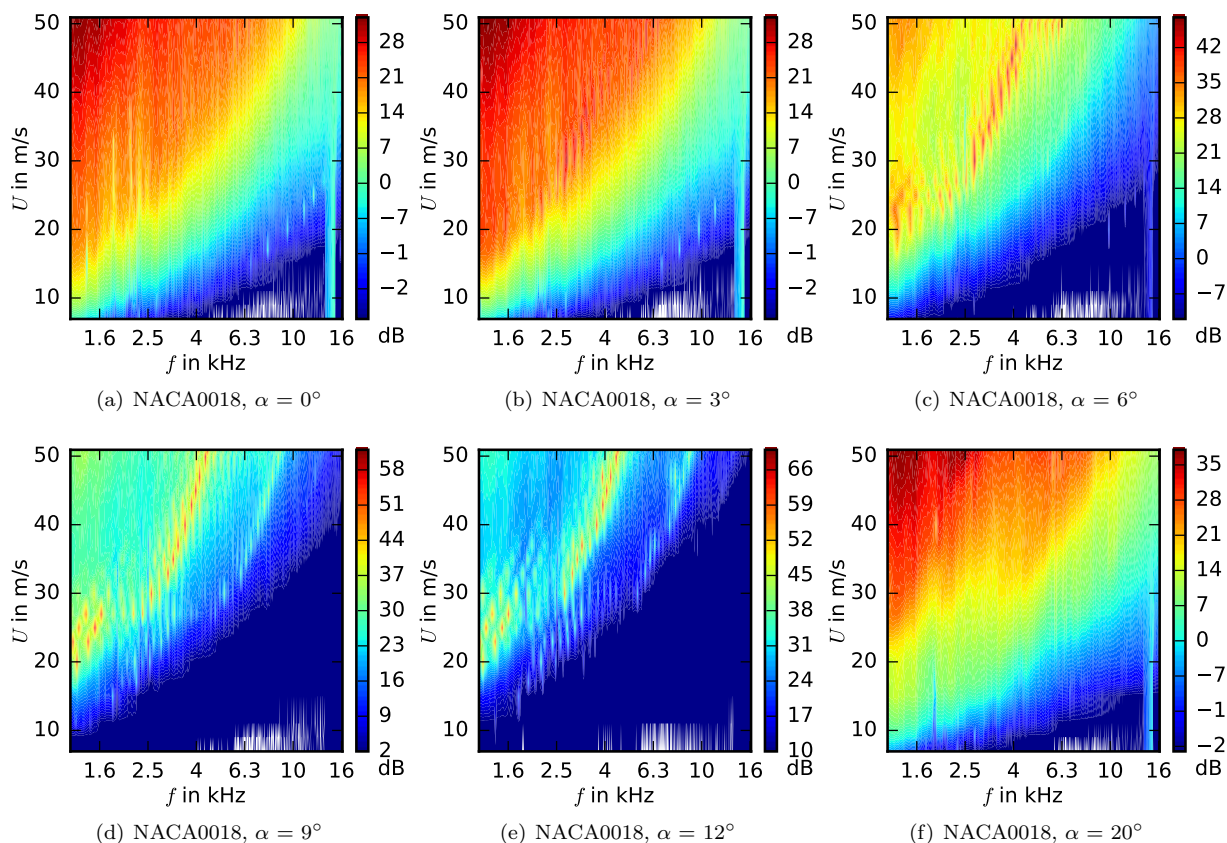


Figure 7. Sound pressure level spectra obtained for the NACA0018 airfoil at different angles of attack as a function of flow speed and frequency

tip where no wall pressure sensors are positioned. The wall pressure spectra of the NACA0018, which does not generate tonal noise at $\alpha = 0^\circ$ (Figure 7(a)), do not feature any narrowband spectral peaks.

At an angle of attack of 6° the surface pressure spectra obtained on the suction side of the NACA0012 airfoil show a set of very thin peaks in a frequency range between 2 kHz and 4 kHz for flow speeds greater than approximately 25 m/s, which agrees well with the tones seen in the corresponding spectral map shown in Figure 6(c). The sound maps for this frequency range show a noise source stretched along a large portion of the trailing edge, including the midspan region (Figure 10). The wall pressure spectra obtained for the NACA0018 at this angle are broadband in character, but very small spectral “ripples” can be seen around 4 kHz for the highest flow speeds. The sound pressure level spectra for this case showed a set of equispaced tones of smaller amplitude (Figures 5 and 7(c)), which are generated by a noise source located at the trailing edge, stretching approximately from mid-span to the tip of the airfoil. Since this source barely extends over the mid-span region of the airfoil, it seems likely that the wall pressure sensors located there do not receive much of the tonal characteristics and hence only show these very thin peaks of low amplitude.

When the angle of attack is further increased to 12° and 20° , the pressure fluctuations of the NACA0012 do not feature any narrowband characteristics, which is in agreement with the fact that at these angles only broadband noise is radiated (shown in Figure 6(e) and 6(f)). The NACA0018 does generate strong tonal noise at an angle of 12° (Figure 7(e)), which is generated by a trailing edge noise source stretched along the entire span (Figure 12). At flow speeds below 30 m/s, the frequency of the tones is in a range between 1 kHz and 1.6 kHz, while at flow speeds above 30 m/s the frequency increases to a range between 2.5 kHz and 5 kHz, which represents another rung of the ladder of dominant frequencies. Again, this tonal noise generation is related to sharp peaks in the spectra of the surface pressure fluctuations. Even the jump of the dominant frequency is visible, since at low speeds the peaks appear in a frequency range between 800 Hz and 1.6 kHz and at higher flow speeds the group of peaks shift to a frequency range between approximately

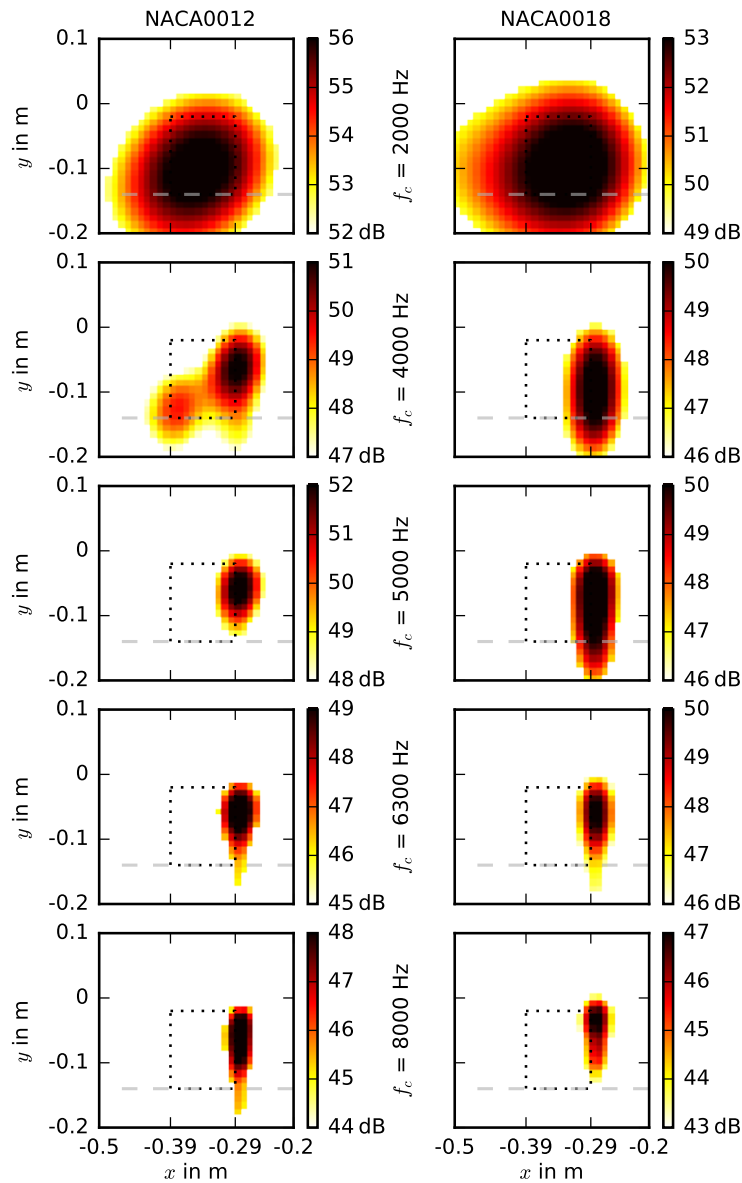


Figure 8. Selected third octave band sound maps obtained at $\alpha = 0^\circ$ and $U = 49.9$ m/s (flow from left to right, dotted black rectangle represents airfoil, dashed gray line represents side wall)

2.5 kHz and 5 kHz. At a geometric angle of attack of 20° neither the acoustic maps (Figure 7(f)) nor the wall pressure spectra of the NACA0018 in Figure 15 show any tonal characteristics.

As discussed before, the noise generation of the two airfoils at negative angles of attack is the same as for positive angles of the same absolute value. However, since wall pressure spectra were only measured at one side of the airfoil, the analysis of the wall pressure spectra measured at negative angles allows for conclusions on the flow over the pressure side of the airfoil. Thus, Figure 16 exemplarily shows wall pressure fluctuations obtained at negative angles of attack of -6° , -12° and -20° .

As expected, differences are visible between the results for the suction side (Figure 15) and those for the pressure side (Figure 16). At -6° the NACA0012 again shows noticeable tonal characteristics. At flow speeds below 20 m/s, those appear as a set of several small, equispaced peaks, while at the highest flow speeds only a single, very thin peak is visible (comparable to those observed at 6° angle of attack, but much smaller in amplitude). The pressure side wall pressure spectra obtained for the NACA0018 at -6° do not show narrowband characteristics. At a geometric angle of attack of -12° , the wall pressure spectra of the

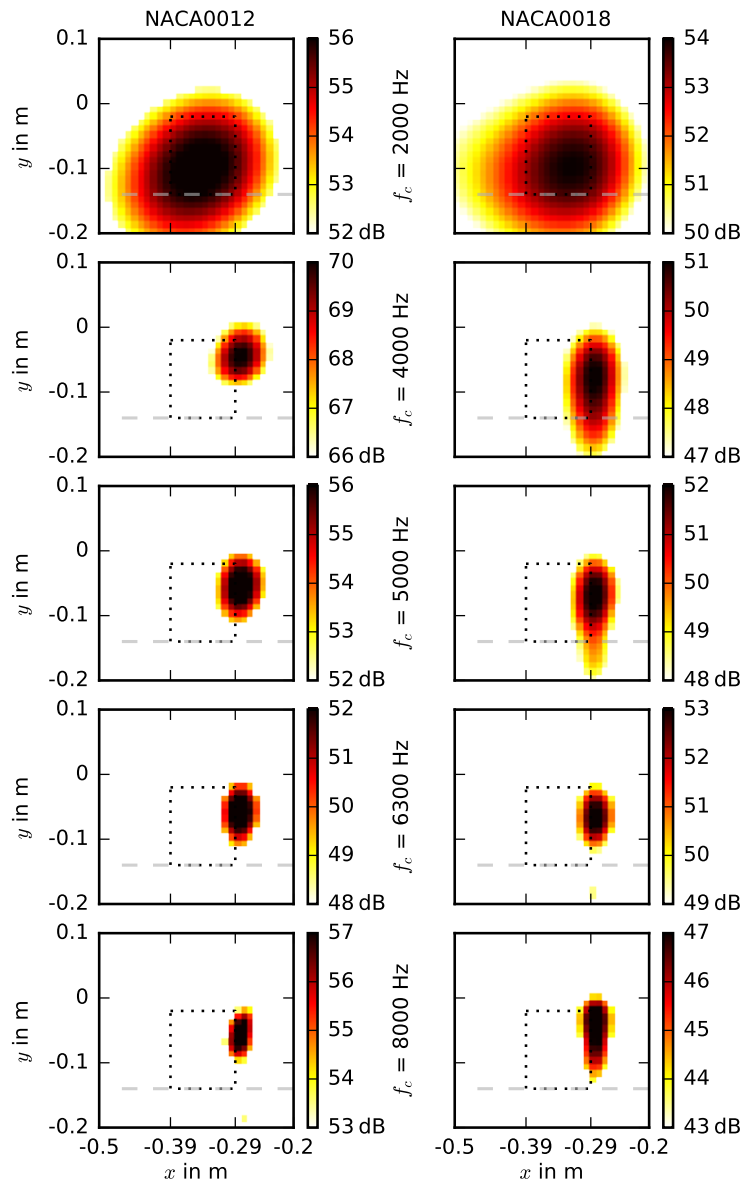


Figure 9. Selected third octave band sound maps obtained at $\alpha = 3^\circ$ and $U = 49.9$ m/s (flow from left to right, dotted black rectangle represents airfoil, dashed gray line represents side wall)

NACA0012 have more or less broadband character, while thin spectral peaks are visible for the NACA0018 airfoil. This is basically similar to the observation made at an angle of 12° . Finally, at -20° neither the wall pressure spectra of the NACA0012 nor that of the NACA0018 show any tonal characteristics, which is again similar to the results seen for the suction side at 20° angle of attack.

In order to further examine the relation between wall pressure spectra and acoustic results regarding the generation of tonal noise, wall pressure spectra from the sensors farther away from the trailing edge will be examined for selected angles and flow speeds. Two cases that are of particular interest are the NACA0012 at zero angle of attack at a low flow speed and at a high flow speed. In the first case, the wall pressure spectra obtained by the sensor closest to the trailing edge contained noticeable narrowband maxima, while in the second case the spectra had broadband character.

As an example for the first case, Figure 17 shows the wall pressure spectra obtained by all six sensors as well as the coherence γ^2 between the first five sensors (at $x/c_l = 0.2, 0.32, 0.44, 0.56, 0.68$) with the sensor 6 closest to the trailing edge (at $x/c_l = 0.8$) for both airfoils at zero angle of attack and a low flow speed of

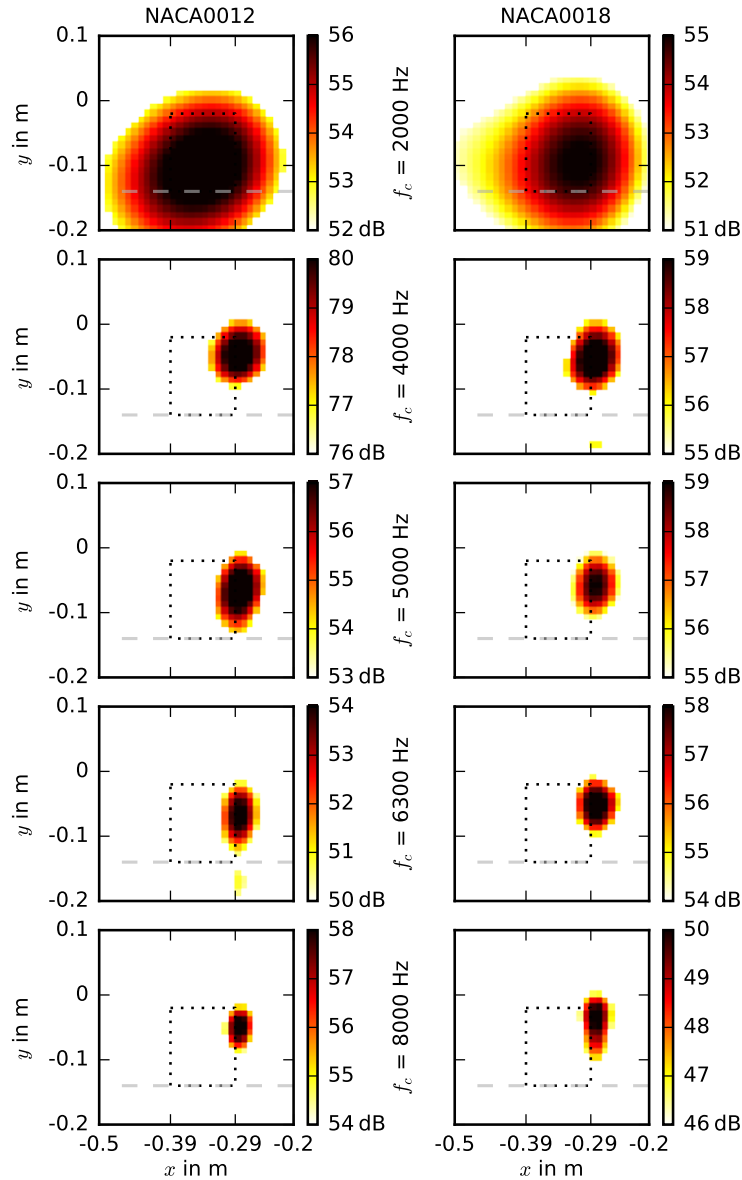


Figure 10. Selected third octave band sound maps obtained at $\alpha = 6^\circ$ and $U = 49.9$ m/s (flow from left to right, dotted black rectangle represents airfoil, dashed gray line represents side wall)

11 m/s. It can clearly be seen that the peaks in the wall pressure spectra of the NACA0012 airfoil between 500 Hz and 600 Hz have a very high coherence with the signal obtained by the sensor closest to the trailing edge (Figure 17(a)). This means that the instabilities related to these peaks already form close to the leading edge and are then transported downstream (where they lead to the generation of tonal noise when scattered at the trailing edge). The spectra obtained for the NACA0018 at the same angle of attack and flow speed (Figure 17(b)) do not show notable narrowband characteristics, and hence the coherence between the signals obtained from the first five wall pressure sensors with the one closest to the trailing edge is low.

This theory is somewhat confirmed by Figure 18, which shows the wall pressure spectra from all sensors as well as the coherence again at an angle of attack of 0° , but at a much higher flow speed of 49.9 m/s. At this flow speed, both airfoils generate only broadband noise without any tones (see Figures 6(a) and 7(a)), which is in agreement with the broadband character of the wall pressure spectra of the sensor closest to the trailing edge at this flow speed (Figure 15). Accordingly, the spectra obtained by the other five wall pressure sensors (at $x/c_l < 0.8$) also show no narrowband features, and the coherence with the sensor closest to the

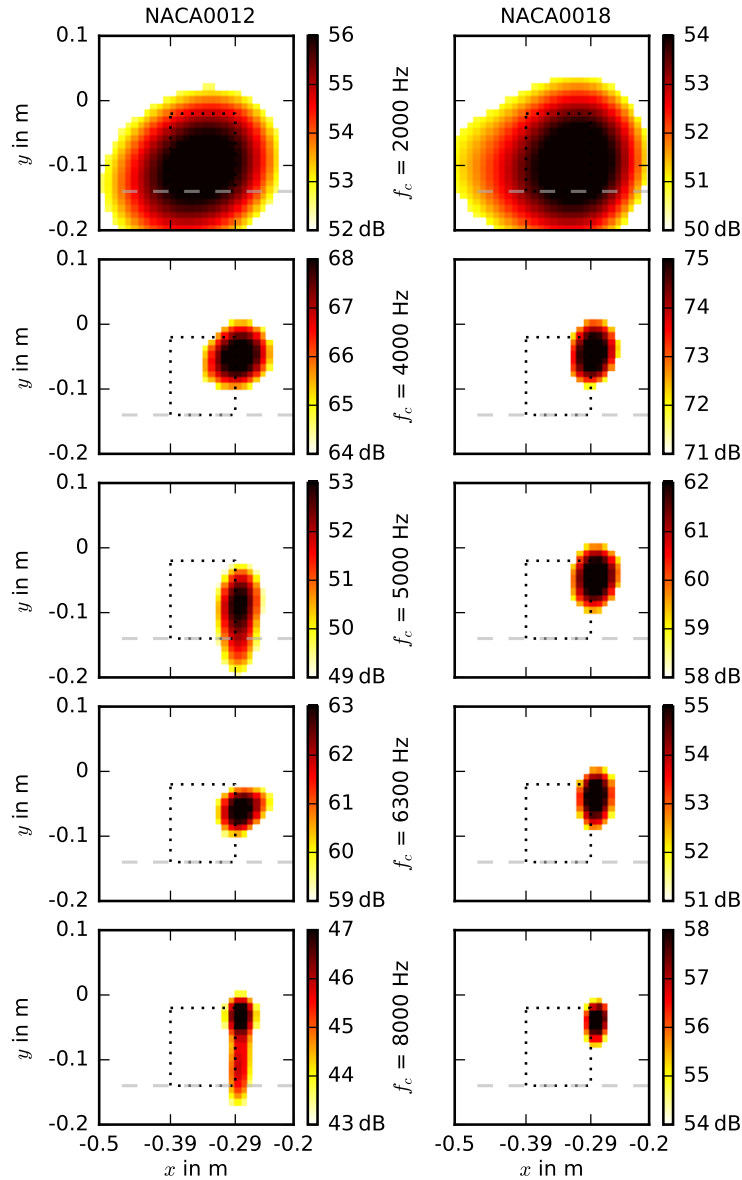


Figure 11. Selected third octave band sound maps obtained at $\alpha = 9^\circ$ and $U = 49.9$ m/s (flow from left to right, dotted black rectangle represents airfoil, dashed gray line represents side wall)

trailing edge is low.

As another example, the wall pressure spectra and the coherence obtained at an angle of attack of 12° and a high flow speed of 49.9 m/s are presented in Figure 19. In this interesting case, the NACA0012 is generating broadband noise only (Figure 6(e)), which is reflected in the broadband character of the wall pressure spectra obtained by the sensor closest to the trailing edge (see Figure 15). Accordingly, the spectra obtained by the three downstream sensors (at $x/c_l = 0.56, 0.68$ and 0.8) do not show tonal characteristics. Only the sensors at the upstream region of the airfoil (at $x/c_l = 0.22, 0.32$ and 0.44) show spectral peaks at high frequencies approximately above 3 kHz. However, the flow instabilities related to these peaks seemingly do not travel downstream or the disturbances are broken up due to transition to turbulence on the suction side at this high angle of attack, and accordingly the coherence of the signals from these sensors with that from the sensor closest to the trailing edge is again very low. At this angle of attack and flow speed, the NACA0018 generates strong tonal noise at a frequency between 4 kHz and 5 kHz (see Figures 5(b) and 7(e)), while the wall pressure spectrum measured close to the trailing edge features corresponding peaks (Figure 15). The

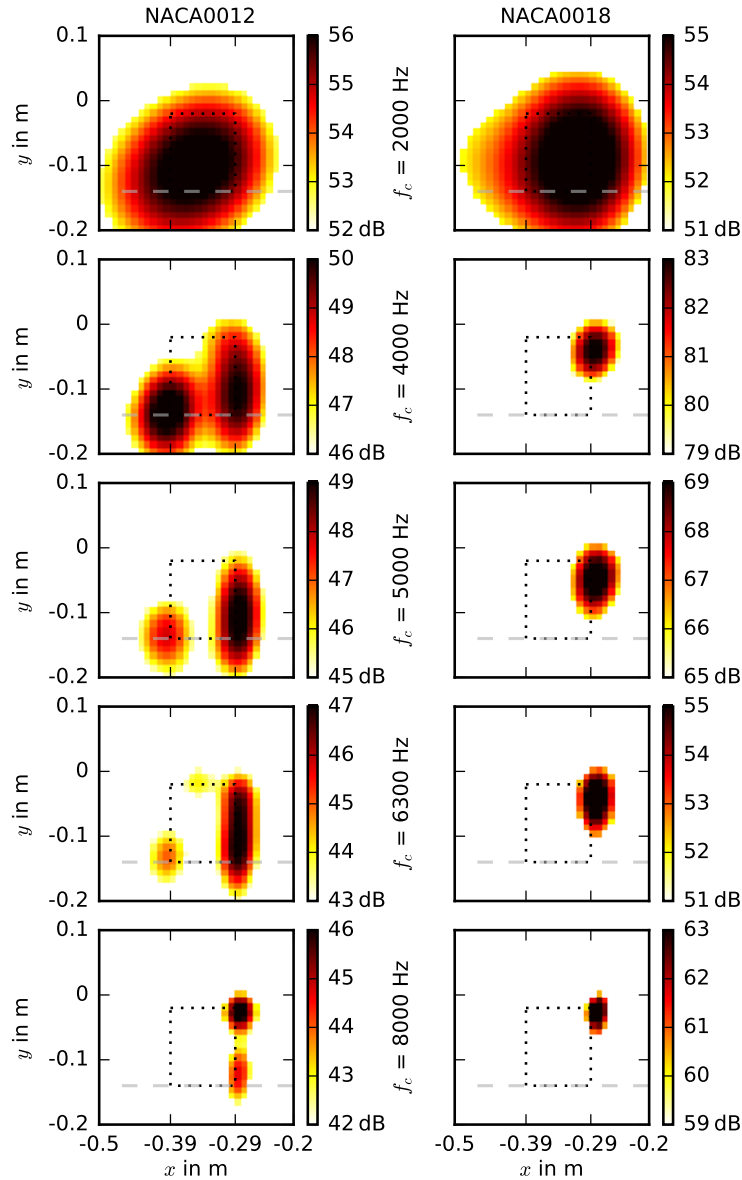


Figure 12. Selected third octave band sound maps obtained at $\alpha = 12^\circ$ and $U = 49.9$ m/s (flow from left to right, dotted black rectangle represents airfoil, dashed gray line represents side wall)

wall pressure spectra obtained by the other sensors also show a peak at this frequency, which is connected to a peak of the coherence with the trailing edge sensor. Again, this can be understood as an instability which develops on the surface of the airfoil close to the leading edge and then travels downstream with the boundary layer, gets scattered at the trailing edge and radiated as tonal noise.

IV. Summary

In order to examine the influence of airfoil thickness on the tonal noise generation of wall-mounted finite airfoils, an experimental study was performed in an open jet wind tunnel on a NACA0012 and a NACA0018 airfoil, which has a nominal thickness of 12 % and 18 % of the chord length, respectively. This included acoustic measurements using a planar microphone array consisting of 47 microphones, measurements of the pressure fluctuations on the surface of the airfoils using six flush-mounted electret capsules and surface flow visualizations.

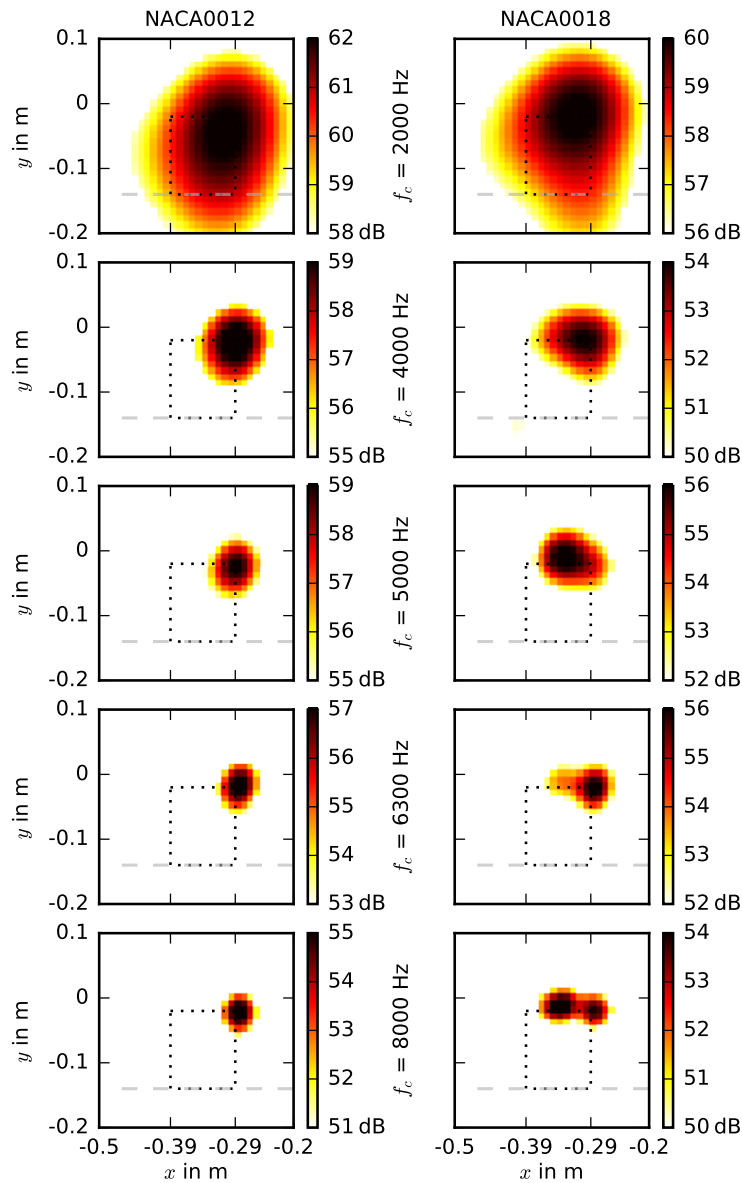


Figure 13. Selected third octave band sound maps obtained at $\alpha = 20^\circ$ and $U = 49.9$ m/s (flow from left to right, dotted black rectangle represents airfoil, dashed gray line represents side wall)

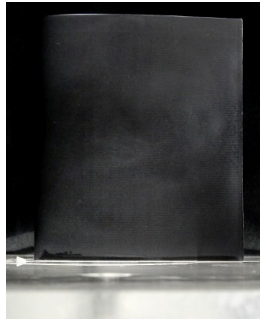
The results show that airfoil thickness has a strong influence on the generation of tonal noise. At high flow speeds and low geometric angles of attack around 6° , the NACA0012 airfoil generates a very strong tone with weaker side tones, while the thicker NACA0018 generates a set of equispaced tones of lower amplitude. When the angle is increased to about 12° , the NACA0012 does not produce notable tonal noise any more, while the NACA0018 now generates a similar strong tone with weaker side tones as the NACA0012 at the lower angle of attack. The existence of these tonal structures is accompanied by spectral peaks of the wall pressure fluctuations, which are highly correlated between sensors at different chordwise positions. In most cases, the tonal noise is generated by a source positioned at a region of the trailing edge close to the free end of the airfoil. At this location, the exemplary flow visualization experiments performed at zero angle of attack revealed a region of flow separation. Future hot-wire measurements are planned to further examine the flow over the trailing edge in this region.

Acknowledgements

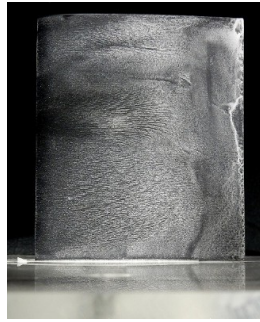
The authors thank Sven Haase for his help with the measurements.

References

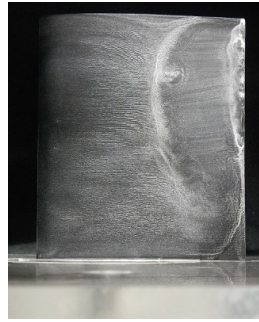
- ¹Brooks, T. F., Pope, D. S., Marcolini, M. A., Airfoil self-noise and prediction NASA Reference Publication 1218, 1989
- ²Paterson, R. W., Vogt, P. G., Fink, M. R., Munch, C. L., Vortex noise of isolated airfoils. *J. Aircraft*, 10(5), 296-302, 1973
- ³Arbey, H., Bataille, J., Noise generated by airfoil profiles placed in a uniform laminar flow. *Journal of Fluid Mechanics*, 134, 33-47, 1983
- ⁴McAlpine, A., Nash, E. C., Lawson, M. V., On the generation of discrete frequency tones by the flow around an aerofoil. *Journal of Sound and Vibration*, 222(5), 753-779, 1999
- ⁵Nash, E. C., Lawson, M. V., McAlpine, A. L. A. N., Boundary-layer instability noise on aerofoils. *Journal of Fluid Mechanics*, 382, 27-61, 1999
- ⁶Brooks, T. F., Marcolini, M. A., Airfoil tip vortex formation noise. *AIAA Journal*, 24(2), 246-252, 1986
- ⁷Moreau, D. J., Prime, Z., Porteous, R., Doolan, C. J., Valeau, V., Flow-induced noise of a wall-mounted finite airfoil at low-to-moderate Reynolds number. *Journal of Sound and Vibration*, 333(25), 6924-6941, 2014
- ⁸Moreau, D. J., Doolan, C. J., Tonal noise production from a wall-mounted finite airfoil. *Journal of Sound and Vibration*, 363, 199-224, 2016
- ⁹Moreau, D. J., Geyer, T. F., Doolan, C. J., Sarradj, E., Camber effects on the tonal noise and flow characteristics of a wall-mounted finite airfoil. 23rd AIAA/CEAS Aeroacoustics Conference, AIAA paper 2017-3172, 2017
- ¹⁰Sarradj, E., Fritzsche, C., Geyer, T. F., Giesler, J., Acoustic and aerodynamic design and characterization of a small-scale aeroacoustic wind tunnel, *Appl Acoust*, 70, 1073-1080, 2009
- ¹¹Sijtsma, P., CLEAN based on spatial source coherence. *International Journal of Aeroacoustics*, 6(4), 357-374, 2007
- ¹²Mueller, T.J. (ed.), *Aeroacoustic measurements*. Springer Science+Business Media, Berlin, 2002
- ¹³Giesler, J., Sarradj, E., Measurement of broadband noise generation on rod-airfoil-configurations. 15th AIAA/CEAS Aeroacoustics Conference, AIAA paper 2009-3308, 2009
- ¹⁴Garcia-Sagrado, A., Hynes, T. Stochastic estimation of flow near the trailing edge of a NACA0012 airfoil. *Experiments in Fluids*, 51(4), 1057, 2011



(a) $Re = 0$ ($U = 0$ m/s)



(b) $Re = 45,900$
($U = 6.9$ m/s)



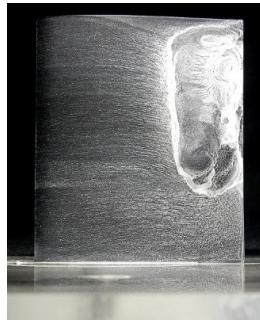
(c) $Re = 59,600$
($U = 9.0$ m/s)



(d) $Re = 72,800$
($U = 11.0$ m/s)



(e) $Re = 99,000$
($U = 15.0$ m/s)



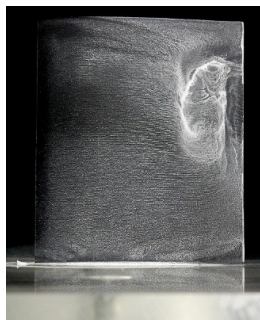
(f) $Re = 132,000$
($U = 20.0$ m/s)



(g) $Re = 165,000$
($U = 25.0$ m/s)



(h) $Re = 198,000$
($U = 30.0$ m/s)



(i) $Re = 231,000$
($U = 34.9$ m/s)



(j) $Re = 264,000$
($U = 39.9$ m/s)



(k) $Re = 297,000$
($U = 44.9$ m/s)



(l) $Re = 330,000$
($U = 49.9$ m/s)

Figure 14. Surface flow visualization for the NACA0012 airfoil at different flow speeds (flow from left to right, wall on bottom)

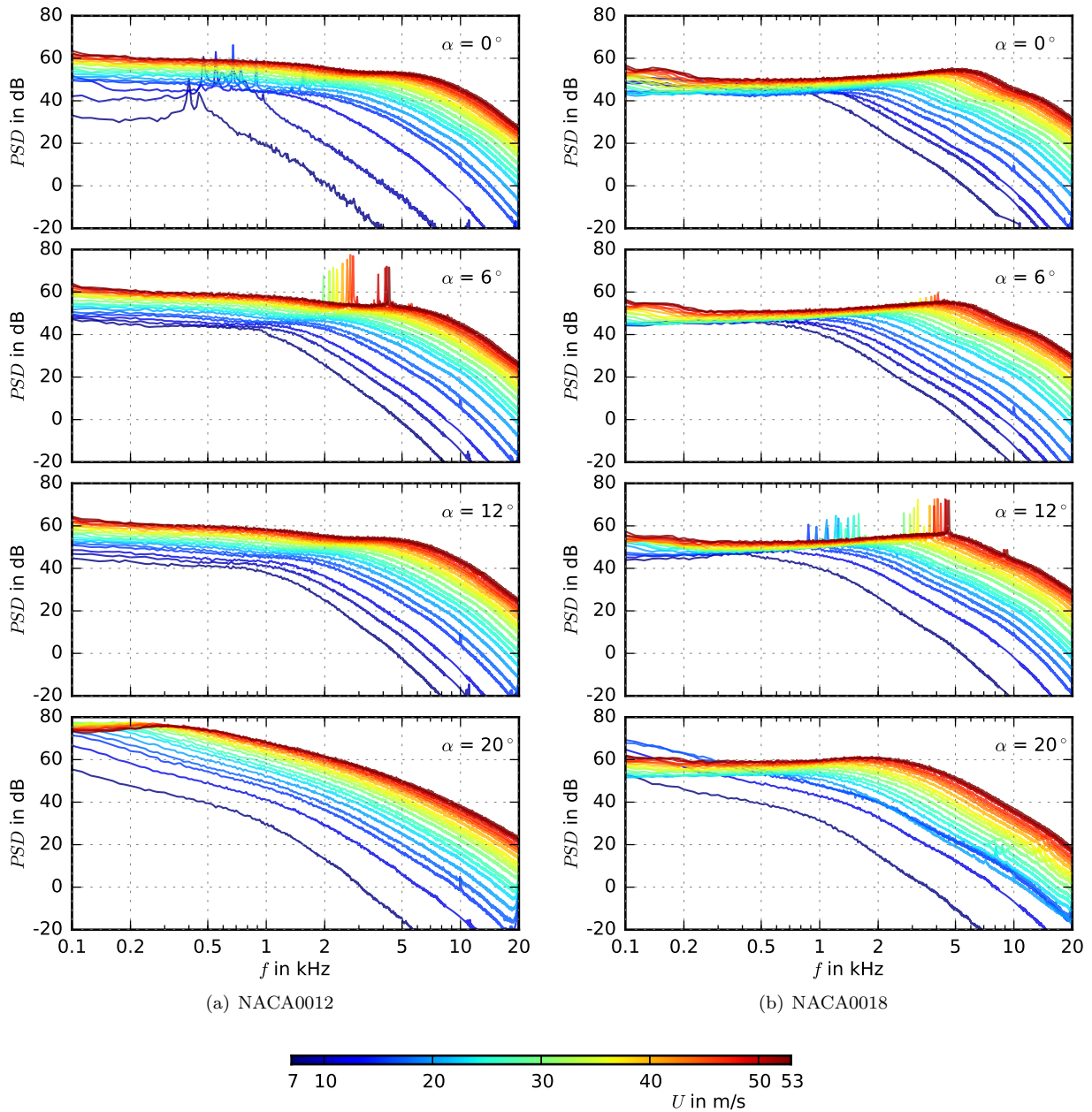


Figure 15. Wall-pressure spectra measured by the sensor closest to the trailing edge ($x/c_l = 0.8$) for different flow speeds U and non-negative angles of attack α (left: NACA0012, right: NACA0018)

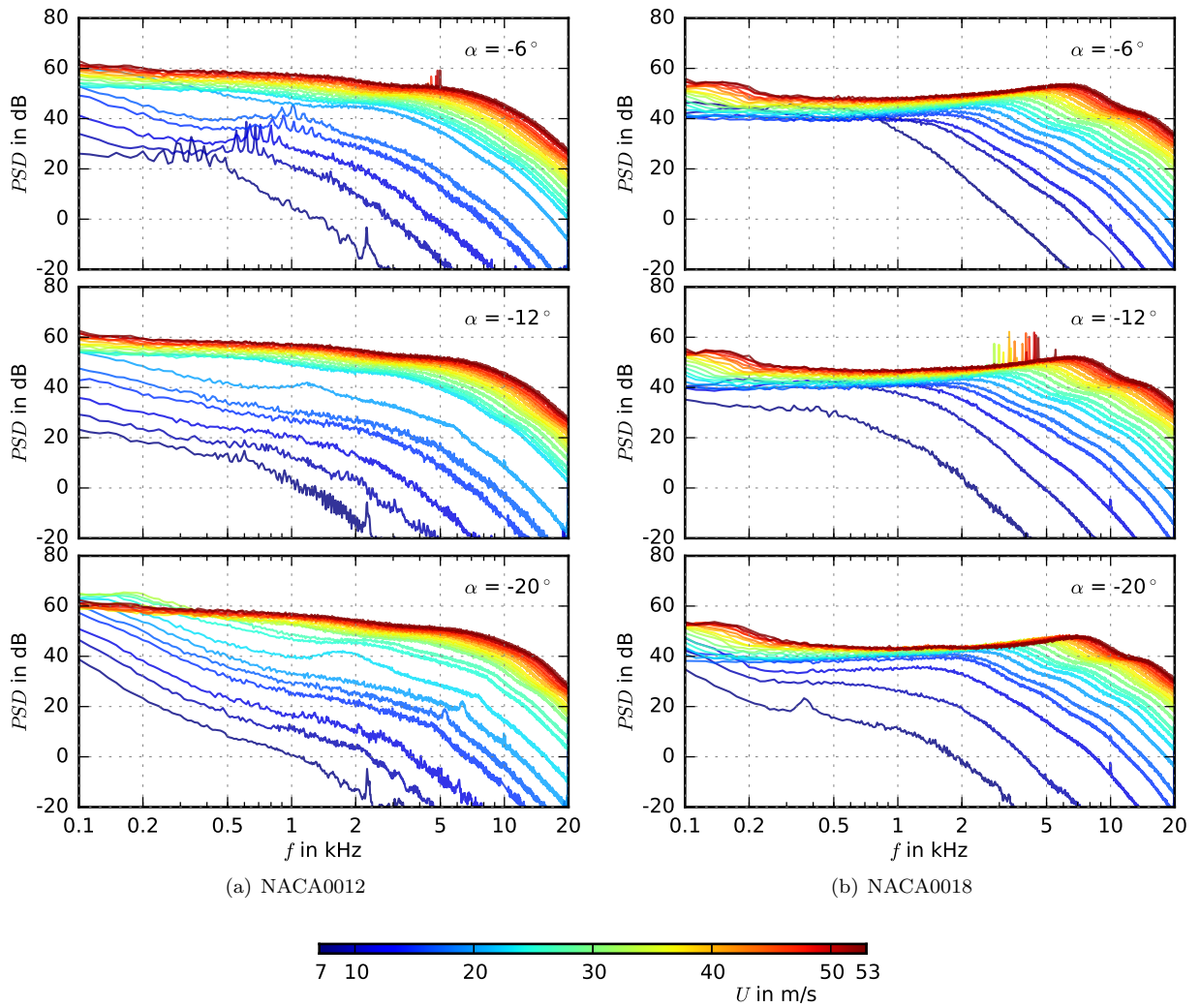


Figure 16. Wall-pressure spectra measured by the sensor closest to the trailing edge ($x/c_t = 0.8$) for different flow speeds U and negative angles of attack α (left: NACA0012, right: NACA0018)

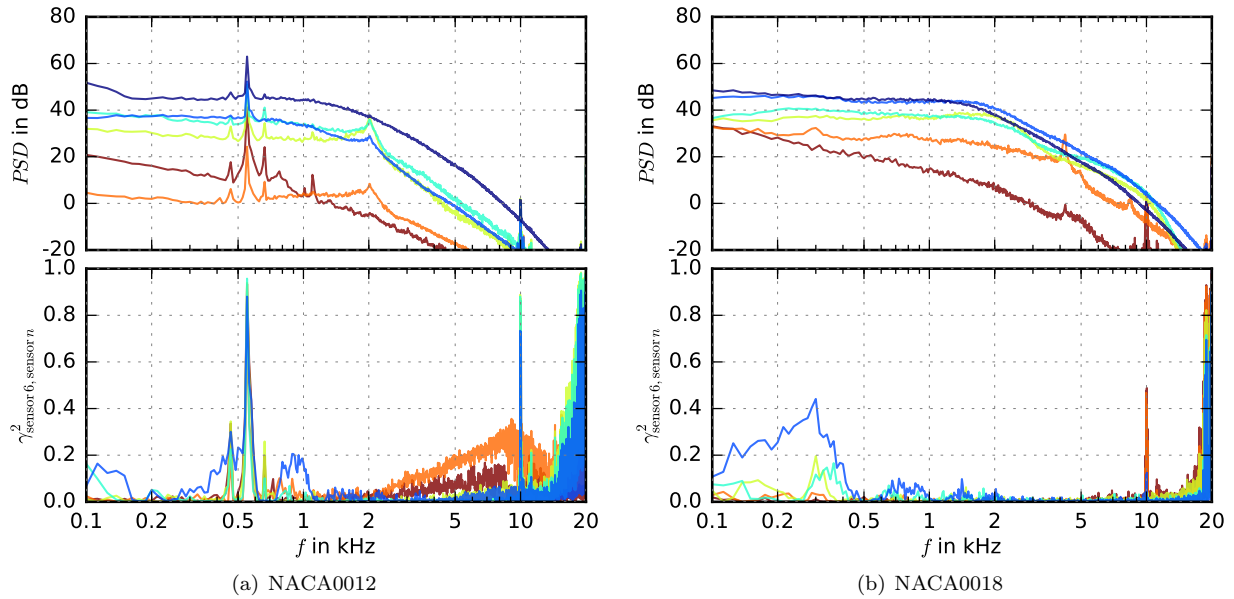


Figure 17. Wall-pressure spectra measured by all sensors (top) and coherence between all sensors at $x/c_l < 0.8$ with the one closest to the trailing edge at $x/c_l = 0.8$ (bottom) for a low flow speed of 11 m/s and zero angle of attack (left: NACA0012, right: NACA0018), $x/c_l =$ ■ 0.2, ■ 0.32, ■ 0.44, ■ 0.56, ■ 0.68, ■ 0.8 (Note that the narrow peak at $f = 10$ kHz is not generated by the flow, but is an artefact from the signal processing electronics.)

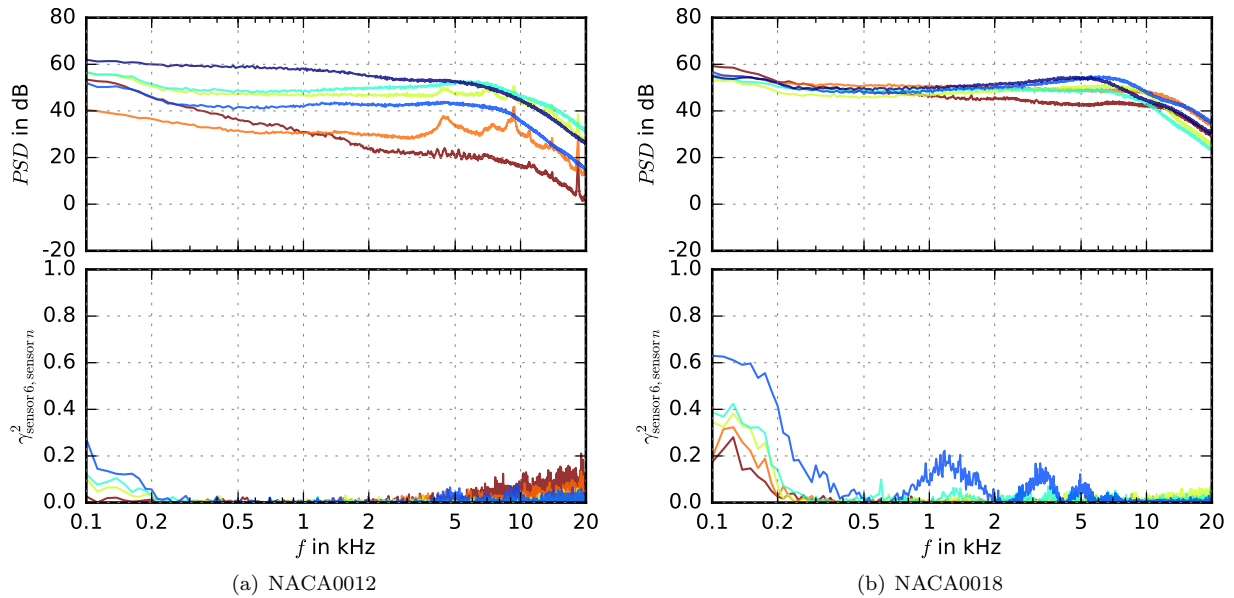


Figure 18. Wall-pressure spectra measured by all sensors (top) and coherence between all sensors at $x/c_l < 0.8$ with the one closest to the trailing edge at $x/c_l = 0.8$ (bottom) for a high flow speed of 49.9 m/s and zero angle of attack (left: NACA0012, right: NACA0018), $x/c_l =$ ■ 0.2, ■ 0.32, ■ 0.44, ■ 0.56, ■ 0.68, ■ 0.8

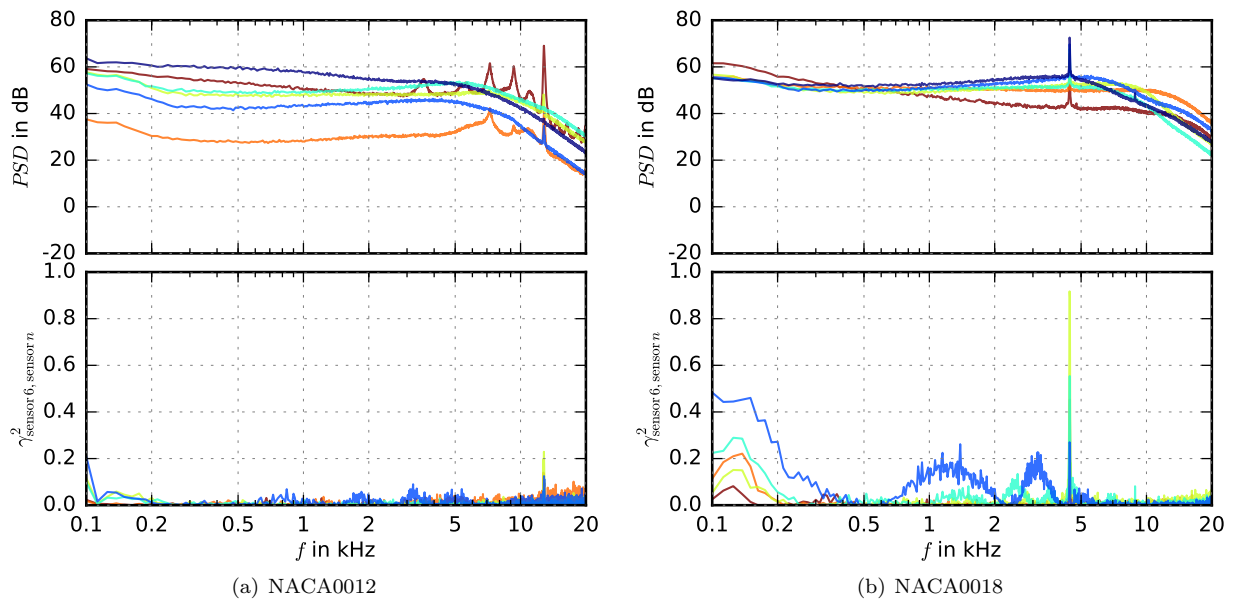


Figure 19. Wall-pressure spectra measured by all sensors (top) and coherence between all sensors at $x/c_l < 0.8$ with the one closest to the trailing edge at $x/c_l = 0.8$ (bottom) for a high flow speed of 49.9 m/s and 12° angle of attack (left: NACA0012, right: NACA0018), $x/c_l =$ ■ 0.2, ■ 0.32, ■ 0.44, ■ 0.56, ■ 0.68, ■ 0.8